

1 Observations of Sea Ice Melt from Operation IceBridge Imagery

2 Nicholas C. Wright¹, Chris M. Polashenski^{1,2}, Scott T. McMichael³, Ross A. Beyer^{3,4}

3 ¹Thayer School of Engineering, Dartmouth College, Hanover, NH, USA

4 ²U.S. Army Cold Regions Research and Engineering Laboratories, Hanover, NH, USA

5 ³NASA Ames Research Center, Moffet Field, CA, USA

6 ⁴SETI Institute, Mountain View, CA, USA

7

8 *Corresponding author:* Nicholas Wright (ncwright.th@dartmouth.edu)

9 **Abstract.** The summer albedo of Arctic sea ice is heavily dependent on the fraction and color of melt
10 ponds that form on the ice surface. This work presents a new dataset of sea ice surface fractions along
11 Operation IceBridge (OIB) flight tracks derived from the Digital Mapping System optical imagery set. This
12 dataset was created by deploying version 2 of the Open Source Sea-ice Processing (OSSP) algorithm to
13 NASA's Advanced Supercomputing Pleiades System. These new surface fraction results are then
14 analyzed to investigate the behavior of meltwater on first-year ice in comparison to multiyear ice.
15 Observations herein show that first-year ice does not ubiquitously have a higher melt pond fraction than
16 multiyear ice under the same forcing conditions, contrary to established knowledge in the sea ice
17 community. We discover and document a larger possible spread of pond fractions on first-year ice
18 leading to both high and low pond coverage, in contrast to the uniform melt evolution that has been
19 previously observed on multiyear ice floes. We also present a selection of optical images that captures
20 both the typical and atypical ice types, as observed from the OIB dataset. We hope to demonstrate the
21 power of this new dataset and to encourage future collaborative efforts to utilize the OIB data to
22 explore the behavior of melt pond formation Arctic sea ice.

Deleted:

24 **1 Introduction**

25 The extent and age of the Arctic sea ice cover has declined since the beginning of the satellite record in
26 1979 (Stroeve et al., 2012). Ice melt is accelerated through albedo feedback cycles initiated by surface
27 melt decreasing the ice cover’s reflectance (Curry et al., 1995; Perovich et al., 2003). Understanding
28 changes in sea ice properties that impact albedo, particularly melt pond coverage, is important to
29 parameterizing sea ice in global climate models (Hunke et al., 2013; Serreze et al., 2009). In-situ
30 observations that could support developing this understanding are sparse, difficult to acquire, and may
31 not be broadly representative (Perovich, 2002a; Wright and Polashenski, 2018). Remote sensing
32 platforms provide a path to understanding sea ice surface change over larger scales. Newly developed
33 computational techniques provide the means to analyze large remotely sensed datasets (Miao et al.,
34 2015; Webster et al., 2015; Wright and Polashenski, 2018). The NASA Operation IceBridge project (OIB)
35 has collected large amounts of high-resolution optical imagery of sea ice with the Digital Mapping
36 System (DMS) (Dominguez, 2010, updated 2017). At ~10cm resolution, these images capture the ice
37 surface in fine detail – but it is challenging to convert them to quantitative measures of ice conditions.

Deleted: exquisite

38 A new technique for analyzing high-resolution optical imagery of sea ice has recently been
39 developed and demonstrated (Wright and Polashenski, 2018). This technique, named the Open Source
40 Sea-ice Processing algorithm (OSSP), automatically analyzes input imagery and classifies image area into
41 four primary surface type categories: 1) snow and unponed ice, 2) dark or thin ice, 3) melt ponds and
42 submerged ice, and 4) open ocean, Categories 1 and 2 are often combined to create a unified ice
43 category. Several improvements and new features that define version 2 of OSSP are presented here.
44 This version was used to create a new dataset by deploying the algorithm on a large scale to process the
45 entirety of the NASA OIB optical image dataset. This dataset is now publicly available for community use
46 and for other studies leveraging the IceBridge data suite. This publication is intended partially to serve
47 as supporting documentation for those uses.

Deleted: three

Deleted: 3

Deleted: s such as melt ponds, unponed ice, and open ocean

Deleted:

48 The summer portion of the new dataset is then used to evaluate existing hypotheses about melt
49 pond formation on Arctic sea ice. One such hypothesis describes the prevalence of ponds on first-year
50 sea ice (FYI) versus multiyear ice (MYI). It has been widely stated that FYI has a higher average fractional
51 pond coverage than MYI over the complete melt season (Eicken et al., 2004; Fetterer and Untersteiner,
52 1998a; Morassutti and Ledrew, 1996; Perovich and Polashenski, 2012). This would contribute to positive
53 ice-albedo feedbacks, since the higher pond fraction would lower albedo of FYI, re-enforcing the
54 transition to a younger ice pack. The reasoning most cited for expecting higher pond coverage on FYI is
55 related to ice and snow topography (Barber and Yackel, 1999; Derksen et al., 1997; Eicken et al., 2004).
56 When ice grows from open Arctic waters, it tends to form in flat, undeformed pans or fairly level
57 pancake fields (Weeks, 2010). Though these pans are subsequently broken and ridged by dynamic
58 forces, in most parts of the Arctic a large fraction of FYI remains level. When surface melt begins on level
59 FYI floes, melt water is unconstrained by topography and spreads to cover a large fraction of the surface.
60 On MYI, however, the ice has survived prior melt seasons that create more complex surface topography
61 even in areas without mechanical deformation. The meltwater is then contained by the prior year’s
62 melt-formed topography into well-defined pools. The result should be that FYI would tend to experience
63 greater pond coverage than MYI. Indeed, this has been presented by several authors as a likely change
64 in the Arctic (Eicken et al., 2004; Polashenski et al., 2012).

Deleted: hypothesized

Deleted: a

Field Code Changed

Deleted: a

Deleted: sea

Deleted: in the relatively calm

Deleted: . Prior melt

Deleted: s

Deleted: first-year ice

Deleted: multiyear ice

Deleted: posited

Deleted: a

81 It is important to note that pond evolution over the melt season is highly variable and is controlled
 82 by the balance of melt water inflow and outflow rates, surface topography, and snow depth. There are
 83 four stages that characterize seasonal melt pond formation described in Eicken et al. (2002) and
 84 paraphrased as follows: (1) Initial onset of ponds above sea level with a rapid increase in areal coverage,
 85 (2) increased outflow allowing drainage to sea level with a decline in areal extent, (3) graduate increase
 86 in areal coverage due to ice melting to below ocean freeboard, and (4) refreezing. Despite a common
 87 understanding of high pond coverage on FYI, a collection of previous observations (Eicken et al., 2004;
 88 Perovich, 2002; Webster et al., 2015) have shown the possibility that FYI has lower pond coverage than
 89 MYI under certain circumstances. For example, in stage 2, areal coverage drops significantly more on FYI
 90 than it does on MYI (Polashenski et al., 2012). Observations at the SHEBA drifting ice camp found that
 91 10-30% of the FYI in the region formed few melt ponds. Measurements there linked this observation to
 92 snow cover: Ice with little or no snow cover and with more than 0.5m snow cover had less than 1% pond
 93 coverage (Eicken et al., 2004). Webster et al., (2015) found regions where FYI started ponding much
 94 later than MYI, though the FYI ultimately developed higher pond coverage later in the summer. A new
 95 observational dataset of melt ponds on sea ice from OIB is used here to assess pond coverage
 96 differences between ice age at the height of summer melt (July), and to expand previous observations of
 97 pond-free FYI to regional scales.

98 A second, related, hypothesis on the behavior of FYI melt ponds suggests two summer melt
 99 evolution pathways exist: one which yields high pond fraction, and one that yields near-zero pond
 100 fraction (Perovich, 2002a; Polashenski et al., 2017), depending on early season ice permeability and the
 101 duration of surface flooding. Our new observations of pond coverage over large areas of FYI provide
 102 additional insight. Here, the OSSP-labeled OIB images were used to assess the variation in pond
 103 coverage on FYI and the prevalence of pond-free floes within the Chukchi and Beaufort Seas. To
 104 accomplish this, a method of post-processing has been developed that determines the size of sea ice
 105 areas devoid of pond coverage as a metric to quantitatively address the prevalence of low pond
 106 coverage. This new analysis reveals that FYI pond coverage indeed exhibits both pathways, but that
 107 there is *not* a strict duality – FYI pond coverage appears to occupy all states across the near-zero to high
 108 coverage space. While the OIB image dataset provides large spatial coverage over long flight transects,
 109 the lack of temporal coverage makes it impossible to directly link these snapshots of pond coverage to
 110 any specific pond evolution process.

111 2 Methods

112 2.1 Data Sources

113 The datasets described herein are the result of processing NASA Operation IceBridge optical DMS
 114 imagery. The DMS images were acquired with a Canon EOS 5D Mark II digital camera which has a 10cm
 115 horizontal ground resolution and a spatial footprint of ~600x400m when used at the survey altitude of
 116 1500 feet (Dominguez, 2010, updated 2017), and is available for download at the National Snow and Ice
 117 Data Center (NSIDC). 87 IceBridge flights were processed, occurring between 2010 and 2018. The OIB
 118 flights were categorized into freezing and melting conditions, which map to the spring/fall and summer
 119 campaigns respectively. The mean date of melt onset in the Chukchi Sea, Beaufort Sea, and Central
 120 Arctic from 1979-2012 was May 17, May 28, and June 10 respectively (Bliss et al., 2014). Spring flights
 121 took place before these dates (March to mid-May, typically), and summer flights well after (mid to late

- Deleted:
- Deleted: ¶
- Formatted: Not Highlight
- Deleted: , influenced by
- Deleted: general
- Deleted: (
- Deleted: ,
- Formatted: Not Highlight
- Formatted: Not Highlight
- Deleted: i
- Deleted: ¶
- Deleted: this
- Deleted: the
- Deleted: general
- Deleted: er
- Deleted: b
- Deleted: may actually
- Deleted: ve
- Deleted: I
- Deleted: 2,
- Deleted: (
- Deleted: Polashenski and Eicken)
- Deleted: .
- Deleted: (Perovich, 2002; Webster et al., 2015).
- Deleted: >
- Deleted: areas
- Deleted: at
- Deleted: The
- Deleted: test
- Deleted: this more generally
- Deleted: s
- Deleted: revealing
- Deleted: new evidence that FYI *often* has lower melt pond fractions than neighboring multiyear ice.
- Formatted: Font: Italic

Deleted: is

155 July). No flights took place during melt or freeze onset transitional phases, making this a clean
156 categorization: The flights between March and May were categorized as freezing condition flights (no
157 melt ponds expected), and those taken in July were categorized as melting condition flights (melt ponds
158 expected). One flight during fall freeze-up (October 5) was processed and was grouped with the spring
159 set. Using this delineation, there were 9 flights during melting conditions and 78 flights during freezing
160 conditions. Of the 9 melting condition flights, 4 occurred in 2016 originating from Utqiaġvik, Alaska, and
161 4 occurred in 2017 originating from Thule AFB, Greenland. There was an additional summer flight
162 departing from Utqiaġvik on July 20th, 2016, that was not processed due to constant cloud cover
163 obscuring the images.

164 A graphic of the flight tracks for all OIB sea ice flights processed, colored by freezing/melting
165 condition status, is presented in Fig. 1. For the majority of this paper, we will focus on the melting
166 season (summer) flights, colored in yellow. Spring data products are posted for use by the community.
167 We anticipate that future analysis of spring flight data will help confirm lead identification in analysis of
168 altimetry data and provide statistics on lead size and spacing and morphology useful to studies of, for
169 example, blowing snow loss to leads or ice dynamics.

170 2.2 OSSP Algorithm Improvements

171 A number of improvements have been made to OSSP since the initial version 1 release described in
172 Wright and Polashenski (2018). These changes can be divided into three categories: 1) Those that alter
173 the algorithms used to classify images, 2) those which add new features, and 3) those which improve
174 code efficiency but do not alter the core methodology. Changes that fall into category (3)
175 reimplemented existing functions for improved performance and decreased computational resource
176 usage. These will not be discussed in detail as they do not change the results.

177 2.2.1 Algorithm Refinements

178 OSSP is an object-based segmentation and classification image processing algorithm. In version 1, edge
179 detection for segmentation was done by applying a Sobel-Feldman filter to the image, amplifying the
180 resulting values to highlight strong edges, and thresholding low gradient value pixels to remove weak
181 edges. The amplification factor and threshold value were both presented as tuning parameters that
182 could control the number and strength of edges to detect in the image. In version 2, image edges are
183 instead found with a Canny edge detector (van der Walt et al., 2014), which has three built-in tuning
184 parameters: A gaussian filter with chosen radius that removes noise from the image, a high threshold
185 which selects strong edges, and a low threshold which defines weak edges. These three parameters can
186 be selected based on the quality of the input image and the degree of segmentation sought. The change
187 in edge detection method does not significantly shift the behavior of the OSSP method but allows the
188 user to better tune the segmentation to specific images. The remainder of the OSSP code uses
189 methodology as presented in Wright and Polashenski (2018).

190 2.2.2 New Features

191 Four new features were added for processing the OIB optical image dataset: 1) An image quality
192 analyzer which flags excessive cloud cover or haze, 2) an automatic white balance correction function, 3)

Deleted: Flights

Deleted: before

Deleted: June 1st

Deleted: late

Deleted: after this date

Deleted: There

Deleted: are

Deleted: were several

Deleted: s

Deleted: which

Deleted: are

Deleted: the pre-June 1st

Deleted: images

Deleted: 8

Deleted: 79

Deleted: 8

209 expanded training datasets specific to OIB images, including shadow detection in spring images, and 4)
210 orthorectification to a flat plane WGS84 spheroid.

211 Clouds and semi-opaque haze are common in OIB imagery. These often partly obscure the surface
212 and prevent accurate image classification. An automated algorithm has been added that detects
213 obscured images so that they can be removed from analysis. The quality check is based on applying a
214 Fourier transformation to the image to detect the ratio of high and low frequency features. It is an
215 implementation of the De and Masilamani (2013) method, where the quality score is the percent of
216 image pixels that have a frequency greater than 1/100,000th of the maximum frequency. Poor quality
217 images were empirically found to have a score of less than 0.025, potentially unusable images had a
218 score between 0.025 and 0.035, and images with a score greater than 0.035 were generally acceptable.

219 A large number of OIB images are taken in poor surface lighting conditions. This is often a result of
220 the aircraft flying under cloud cover or high solar zenith angles. Darker than expected and blue-shifted
221 images are observed under these conditions. Unlike the hazy images flagged by the quality check, these
222 can still be accurately classified. An automatic white balance correction function has been added to
223 standardize the hue and exposure of these images and the resulting image classification. We use a
224 single-point white balance algorithm:

$$225 \quad \begin{bmatrix} R_c \\ G_c \\ B_c \end{bmatrix} = \begin{bmatrix} \frac{omax}{R_w} & 0 & 0 \\ 0 & \frac{omax}{G_w} & 0 \\ 0 & 0 & \frac{omax}{B_w} \end{bmatrix} * \begin{bmatrix} R \\ G \\ B \end{bmatrix}$$

226 where

$$227 \quad \text{omax} = \max (R_w, G_w, B_w)$$

228 and (R_w, G_w, B_w) is a chosen white reference pixel, (R, G, B) is the original pixel value triplet, and
229 (R_c, G_c, B_c) is the corrected pixel value triplet. The reference point triplet is chosen automatically based
230 on the image histogram of each color band; it is the smallest value that is both larger than the highest
231 intensity peak and has less than 15% of that peak's pixel counts. This method sets the selected reference
232 point to true white (255,255,255). All other pixels in the image are corrected with the same linear
233 scaling which serves to both adjust the image exposure and rebalance the RGB ratios. The white
234 reference pixel is limited to a minimum value of 200 for images with only a single surface. This prevents
235 them from being improperly stretched so that an open water only image will remain black. The effect
236 this color correction has on two poorly illuminated images is shown in Fig. 2.

237 The OIB dataset has a clear binary division between flights where melt ponds are expected (July),
238 and those where they are not (March–May). This characteristic allows for the utilization of two
239 specialized training datasets—one for each season. The summer training dataset is a new, larger, set than
240 was presented along with OSSP v1.0, including additional points to encompass a wider range of possible
241 ice conditions. The spring training dataset includes a ridge shadow surface classification class and does
242 not include a melt pond category. The shadow detection method was not applied to melting condition
243 images as the typical summer solar zenith angle yields fewer shadows. The algorithm allows melt pond
244 and shadow detection to be used together given the correct training data, but this was not utilized for
245 the creation of the dataset described here. Webster et al., (2015) found that ridge shadows make up less

Deleted: Limits to the scaling are in place to prevent images

Deleted:

Deleted: (e.g.

Deleted:)

Deleted: this

Deleted:

Deleted: spring and summer flights

253 [than 0.5% of the ice surface in spring, indicating that any errors due to misclassifying them are small.](#)
254 Removal of the melt pond category from spring images prevented occasional spurious detection of melt
255 ponds and improved the quality of results. The training data creation followed the same technique
256 presented in the OSSP version 1.0 documentation (Wright and Polashenski, 2018). The summer dataset
257 was expanded to a total of 1706 training points, and the spring dataset to a total of 865 points. These
258 training datasets can be found along with the OSSP code at (<https://github.com/wrightni/ossps>).

259 2.3 Detecting Pond-Free Ice Areas

260 The labeled image output by the OSSP algorithm was further analyzed to extract metrics about the
261 spatial distribution of water features in summer. [A technique was developed to find contiguous regions](#)
262 [of pond-free ice. These regions were defined as a circle with diameter greater than 12m that does not](#)
263 [overlap any water feature.](#) First, the labeled image was converted into a binary image separating the
264 snow and ice features from water (i.e. melt ponds plus ocean). Next, the distance from every snow/ice
265 pixel to the nearest water feature was calculated, and peaks with a local maximum distance above a
266 threshold of 12 meters were recorded. Pond free areas are [the circle centered at these peaks with a](#)
267 [radius of the distance to the nearest water feature.](#) Any two overlapping regions were combined by
268 adding the non-overlapping area of the smaller region to that of the larger region. These pond free
269 regions are divided into two categories, small and large, based on a threshold of a 2.5 m radius. [The](#)
270 [thresholds of 12m and 25m were selected to be approximately 2x and 4x the mean caliper diameter of](#)
271 [melt ponds](#) (Huang et al., 2016). The number of pond free areas per image was multiplied by the ice
272 fraction (sum of all non-ocean categories) of that image to account for differing ice concentrations
273 between images. Figure 3 shows an example of this detection, where the location of both the small and
274 large regions are marked with small dots and the large regions have a translucent circle showing the size
275 of that region.

276 2.4 Error

277 There are several sources of error in OSSP ice type classifications when applied to the DMS dataset.
278 The established accuracy of the OSSP method, on a high-quality input image, is 96% (Wright and
279 Polashenski, 2018). The principle source of error novel to this OIB dataset was due to lower quality
280 images, typically from haze obscuring the surface or poor surface illumination. While automated
281 methods standardize the quality of the input and flag bad images (Section 2.2.2), some input errors
282 remain. The impact of uncorrected haze is twofold: First, it causes the algorithm to misclassify open
283 water as melt pond, and second, it obscures surface type boundaries and causes insufficient image
284 segmentation. Both issues can be understood by looking at how haze changes an optical image: It adds
285 noise to the image, tends to brighten the pixel values, and blurs surface features. As the defining feature
286 of open water is its uniform darkness, a layer of haze makes this surface more like a dark melt pond. The
287 blurring impacts the edge detection algorithm used by OSSP and therefore causes a breakdown of the
288 proper delineation of image surfaces. For the analyses of the summer dataset presented herein, images
289 were manually sifted to remove those scenes that were not flagged by the QA analysis, but were still of
290 questionable quality. Due to the heterogenous nature of sea ice, there is a trade-off between accuracy
291 on a specific image and accuracy on the entire dataset – some images flagged as low quality may be
292 usable with [a training dataset tailored to those specific images.](#) Users of this dataset should inspect their
293 region of interest to ensure the image quality meets their desired standard.

Deleted:

Deleted: 5

Deleted: defined

Deleted: as a

Deleted: 7.5

Deleted: targeted

Deleted: processing.

301 3 Results

302 3.1 Melt pond fraction along OIB flight tracks

303 In this paper we focus on presenting results from summer images only. Images from 87 IceBridge flights
304 were processed with the OSSP algorithm representing over 900,000 individual images using the
305 methods described above – these results are available for other investigations at the NSIDC archive.
306 Figure 4 maps the track of every melt season OIB flight and plots melt pond fraction observed along
307 these tracks. Melt pond fraction was calculated as the number of melt pond pixels divided by the total
308 ice area (ice pixels + pond pixels). Images where more than 70% of the area was classified as open water
309 are colored black in Figure 4 but were processed normally. Images that were automatically removed due
310 to a low quality score (section 2.2.2) are colored orange, and images that were manually removed due
311 to low image quality are colored red. In total, 40,672 summer images were analyzed, of which 14,876
312 (36.6%) were flagged with a low quality score, 5,671 (13.9%) were manually removed, and 20,125
313 (49.5%) were kept for this analysis. The July 20th, 2016 flight was not processed because only about 2%
314 (30 total) of the images were haze free. Note both high variation in pond coverage along track and
315 general regional changes between flights. Some additional variation between flights is due to temporal
316 change, for example it appears a summer snow occurred just prior to the July 19, 2016 flight, lowering
317 the observed pond fraction.

318 Figure 5 plots 300km of the along-track melt pond fraction for the July 24th, 2017 flight. This figure
319 illustrates the large variability possible in melt pond fraction along track seen in the first half of the flight
320 (top), with a minimum observed fraction of 10% and spikes to greater than 50%. The second half of this
321 flight (bottom) has a more uniform melt pond fraction of ~20%. Four peaks are highlighted in orange
322 where a large blue pond formed on the MYI (See Fig. 11d). Figure 6a zooms in to a 10km subset of this
323 transect, and the surface corresponding to the orange highlighted section is shown in Fig. 6b. The optical
324 image is the result of stitching 23 DMS images together. The highlighted peak in melt pond fraction
325 occurs on a section of FYI between two multiyear floes. This case follows the prevailing hypothesis about
326 the differences between pond formation on MYI and FYI. The relatively flat FYI section allows melt
327 ponds to spread over the surface more evenly, resulting in a higher melt pond coverage, despite
328 encountering the same atmospheric conditions as the MYI on either side. It is also possible that melt
329 water from the MYI drains to the lower elevation FYI (Fetterer and Untersteiner, 1998a).

330 3.2 Influence of Ice Type on Melt Pond Fractions

331 Each summer transect was categorized into first-year ice, multiyear ice, or mixed ice based on manual
332 inspection of those flight's images. The flights classed as a single ice type had at least 90% (estimated
333 from visual inspection) of that type. Melt pond statistics for single ice type flights are shown as box and
334 whisker plots in Fig. 7, where each flight is colored by its ice type categorization; blue for FYI and green
335 for MYI. In these plots the box outline shows the 75th and 25th percentile, the middle line displays the
336 median, the whiskers show 1.5x the interquartile range, and the red points are outliers. Generally, the
337 2016 flights departing from Utqiagvik, Alaska, observed FYI while the 2017 flights departing from Thule
338 AFB, Greenland, observed MYI. There are three exceptions to this categorization: July 13, 2016 and July
339 19, 2016 contain both ice types, where small pockets of MYI were included in the northern sections of
340 an otherwise primarily FYI region, and flight A on July 25th, 2017 covers FYI. Statistics for the two mixed
341 ice type flights are plotted separately in Fig. 8, where each flight is divided into FY or MY ice categories.

Deleted: 200

Deleted: source

Formatted: Not Superscript/ Subscript

Deleted: as there were not enough usable images in that flight

Deleted: the

Deleted: multiyear ice

Deleted: first-year ice

Deleted: -

Deleted: covered

Deleted: first-year ice

Deleted: covered

Deleted: multiyear ice

Deleted: first-year ice

Deleted: first-year

Deleted: multiyear

356 Figure 7 reveals two insights into the difference in melt pond fractions between FYI and MYI. First,
 357 there is no obvious difference in the median pond fraction between flights, and second, there is more
 358 variance in the pond fractions on FYI. The variance is described by the interquartile range, the mean of
 359 which is 0.1 for the first-year flights and 0.05 for the multiyear flights. In other words, while FYI exhibited
 360 a wider range of possible pond fractions, the average coverage is not observed to be higher than on
 361 MYI. The difference in timing and region between OIB flights precludes drawing general conclusions
 362 about differences in median melt pond fraction between ice types. However, two flights that contained
 363 both FY and MY ice were selected for further analysis to investigate melt pond statistics across ice that
 364 experienced similar forcing conditions: July 19, 2016 and July 13, 2016. The portions of these transects
 365 that depict each ice type were manually determined. Results, delineated by ice type, for these two
 366 flights are shown in Fig. 8. The key observation here is that the two flights show opposite relationships:
 367 On July 19 the FYI has a lower median pond fraction, while on July 14, the FYI has a higher median pond
 368 fraction. Previous work has shown the possibility for FYI to have lower pond cover than MYI at local
 369 scales (i.e. individual floes) (Eicken et al., 2004, Webster et al., 2015). Our results support this
 370 observation and show that it can also happen at regional scales. That pond coverage is more variable on
 371 FYI than it is on MYI suggests that while ponds evolve differently on each type there is not a simple
 372 relationship in mean pond fraction. In other words, one cannot conclude that FYI has either higher or
 373 lower pond fractions than MYI.

374 3.3 Observations of Pond-Free First-year Ice

375 The frequency at which FYI develops very low pond coverage was investigated using the pond-free
 376 region detection algorithm to find large unponded areas. Figure 9 shows the results of applying this
 377 algorithm to selected segments of the July 19, 2016 flight. Panel (a) shows the results for a portion of
 378 primarily FYI with high pond coverage, (b) shows a region of FYI that has many areas of pond-free ice,
 379 and (c) shows results from a section of MYI. The ice analyzed for Fig. 9a is what we understand would be
 380 considered as a common state for FYI in an advanced state of melt, where ponds have drained to sea
 381 level but a high portion of the ice floe remains below freeboard and yields a uniformly high pond
 382 fraction. This state coincides with the third stage of pond evolution. This contrasts with the FYI analyzed
 383 for Fig. 9b where, while melt ponds are still present, there are large open areas of pond free ice. The
 384 ponds on the MY floe are regularly distributed and the fractional pond coverage shows little variance.
 385 This could coincide with stage 2 of pond evolution, where ponds have drained and none remain above
 386 freeboard, or to a region where ponds never formed. A timeseries would be required to distinguish
 387 these paths. Expanding from these regions of this specific flight, 17% of all summer FYI images processed
 388 for this study have 3 or more large pond free regions. This reinforces previous observations by Eicken et
 389 al. (2004) that estimated 10 to 30% of FYI surrounding the SHEBA ice camp had “low or zero pond
 390 cover”. In contrast, in the MYI portion of this dataset, only 5% of images have 3 or more large pond free
 391 regions. While there is a clear difference between the MYI and FYI types, the important observation
 392 here is the large percentage of FYI that has lower than expected pond coverage.

393 3.4 Snapshots of a Summer Sea Ice Cover

394 In processing the Operation IceBridge optical imagery dataset, we have had the unique opportunity to
 395 review a significant library of images detailing different sea ice states, looking at thousands of square km
 396 of sea ice. So few people actually observe the sea ice that notions of what is ‘typical’ or unusual are still

Deleted: first-year ice

Deleted: 1
 However, this comparison may not address the hypothesis that pond coverage is higher on FYI because flight lines occurring over two years and were exposed to unique forcing conditions. To investigate melt pond statistics across ice that experienced similar forcing conditions, two flights that contained both FY and MY ice were selected for further analysis:

Deleted: MYI

Deleted: lower

Deleted: These observations confirm FYI can exhibit a lower pond fraction than multiyear ice under similar atmospheric forcing conditions. This suggests that pond evolution on FYI is more variable than on MYI and demands we understand these apparently divergent evolutions.

Deleted: first-year ice

Deleted: first-year ice

Deleted: multiyear ice

Deleted: ‘typical’

Deleted: first year ice

Deleted: by most of the sea ice research community

Deleted: maintain

Deleted: with

Deleted: ____

Deleted: as described in ____

Deleted: our

Deleted: images

Deleted: exhibit pond behavior different from the assumed standard of high coverage.

426 not well known. In this section we present some examples of what we have observed to be
427 'representative' ice states, and examples of ice conditions that are uncommon. These are intended to
428 serve as a qualitative summary of the extensive OIB observations, against which future campaigns can
429 be quickly compared. For each presented image we label the noted features based on the frequency at
430 which we have observed them. Along an arbitrary 100km transect of ice in a given melt state; *common*
431 describes a feature that can be expected on more than half of the ice, *occasional* describes features that
432 would be expected to show up 5-10 times, and *infrequent* describes a feature that may present once or
433 twice.

434 Sea ice scenes shown in Fig. 10: **(a)** FYI that shows a wide range of the possible melt pond fractions,
435 ranging from pond free to high pond coverage; *occasional*. **(b)** Highly ponded level FYI scene in early
436 melt, where ice appear as islands in a sea of water. Such ice was *common* in large areas in the Chukchi
437 sea. **(c)** FYI with high pond fraction and very interconnected pond structure. *Common*; this represents
438 the generally understood behavior of FYI. Here we also see that ponds preferentially form towards the
439 middle of the floe leaving a pond-free border around the edge. The floe-edge gradients are particularly
440 strong in this image, the pond-free border is an *occasional* feature. **(d)** Example of a floe where ponds
441 preferentially form away from the edges. These small floes with central ponds were common in broken
442 FYI. **(e)** Shorefast level ice in the Lincoln sea. Ponds have started to drain already, as evidenced by the
443 drainage channels visible throughout the ice. This type of relatively low coverage and consolidated
444 ponds were *infrequent* in the OIB dataset, but may be common of ice in this region. We speculate that
445 deep snow dunes and thick ice are responsible. **(f)** This image shows a region that appears to have had a
446 recent summer snowfall event. The snow serves to fill shallow ponds with slush or to completely cover
447 them and significantly lowers pond fraction – *infrequent in the OIB dataset* as it is dependent on specific
448 weather conditions. **(g)** A *common* example of high pond fraction FYI. **(h)** Flat and thin ice pans that are
449 almost completely covered by melt water, this scene is *common* for late stages of melt on FYI.

450 Sea ice scenes shown in Fig. 11: **(a-c)** *Common* examples of ponded MYI floes with characteristically
451 blue ponds that are well consolidated by surface topography, showing the range of pond fractions that
452 are possible. **(d)** Example of large reservoir-like ponds that were only observed on MYI. These are
453 *occasional* features on large sections of MYI. **(e)** MYI with FYI inclusions from ocean that refroze during
454 the last winter, this is *common* for MYI at lower latitudes, and *occasional* at higher latitudes. In cases of
455 small FYI inclusions in MYI fields like this, the FYI ice is typically darker had has a higher pond coverage.
456 **(f)** An example of low pond coverage MYI – this was *infrequent* in the OIB dataset. **(g+h)** Ponded FYI
457 undergoing drainage, where evidence of previous ponds is still visible. The overall image represents
458 *common* features, but the drainage pattern here is *infrequently* observed, likely due to its short lifespan.

459 4 Discussion

460 4.1 Variation in Pond Coverage on FYI Precludes Simple Relationship with MYI

461 A general consensus in the sea ice community indicates that FYI has, on average, higher melt pond
462 coverage than does MYI. While such an understanding of ponds is not universally held, it is prevalent
463 and represents a testable hypothesis which our results above did not support. However, it should be
464 noted that our dataset represents a single snapshot in time, and while many melt states were observed
465 in this dataset, it is impossible to assess seasonal averages of melt pond coverage here. The reasoning

Deleted: occurs on most or all

Deleted: First year ice

Deleted: first year ice

Deleted: First year ice

Deleted: first-year ice

Deleted: first-year ice

Deleted: First

Deleted: year

Deleted: first-year ice

Deleted: Note that this scene includes some sediment laden ice, which is also *common*.

Deleted: multiyear ice

Deleted: multiyear ice

Deleted: multiyear ice

Deleted: Multiyear ice

Deleted: first

Deleted: -year

Deleted: multiyear ice

Deleted: first year ice

485 for the hypothesis is two part, covering both early season FYI ponding (when meltwater sits on
486 impermeable ice above sea level) and late season FYI ponding (after ponds have drained to sea level). In
487 the early season case, it is argued that with limited topography, a similar volume of meltwater will flood
488 larger areas of FYI than it would cover on rougher MYI. This is supported by observations in early melt
489 stages, which show FYI melt pond coverage in excess of 60%. Such coverage exceeds that seen on MYI at
490 any time (Landy et al., 2014; Polashenski et al., 2012). In the late season case, it has been argued that
491 thinner FYI will have less buoyancy and less ice area above freeboard. In both cases, FYI ponds would be
492 greater than MYI. These effects must be balanced with the times in melt evolution where FYI is expected
493 to have lower MPF. In the early season, MPF on FYI tends drop faster than on MYI because the
494 meltwater is able to drain to sea level at a faster rate (Polashenski et al., 2012), and in the late season
495 pond fractions on thicker FYI would be lower than MYI because the level surface would have fewer
496 depressions that sit below freeboard. (e.g. Figure 10d).

497 An alternate hypothesis about the behavior of FYI ponds emerging in some recent papers is that FYI
498 pond coverage is extremely variable and may have bimodal evolution driven by snow topography and
499 permeability (Perovich, 2002b; Polashenski et al., 2017; Popović et al., 2018). FYI ponds may not form at
500 all under certain circumstances if the ice is highly permeable or lacks snow cover (Polashenski et al.,
501 (2017) and references therein). Other observations show very high melt pond coverage that persists
502 even after ponds drain to sea level (Polashenski et al., 2015). These divergent possibilities of pond
503 behavior raise the possibility of bimodal behavior wherein some FYI would flood extensively and
504 experience more ponding than MYI while other FYI might not pond at all. The image dataset analysed in
505 this study does not support the bimodal hypothesis, but rather supports the idea that FYI pond coverage
506 is highly variable, existing in all states from low to high pond cover. Diurnal effects can also play a large
507 role in the melt pond fraction on FYI by significantly changing surface melt rates on short time scales,
508 and could therefore be a cause of the high variability seen in our dataset. (Eicken et al., 2004; Hanesiak
509 et al., 1999). Understanding the distribution of MPF on basin wide scales would be key to understanding
510 whether the transition from MY to FYI has a net increase on pond prevalence. No large scale,
511 comprehensive observations have been available to resolve how prevalent such behaviors are.

512 Our image dataset provides some such information on the nature of FYI ponding, but has limitations
513 due to each flight being a temporal snapshot. The time covered by the images is late in the melt season,
514 when much of the FYI is fully permeable and ponds, if any formed, have drained to sea level (see
515 Polashenski et al. (2012) or Eicken et al. (2002) for a description of the stages of pond evolution).
516 Evidence of pond drainage features is common, and we conclude the ponds are largely at sea level.
517 Polashenski et al., (2012) showed that ponds remaining after pond levels drain to sea level are simply
518 those areas where the ice surface floats below sea level. The late season pond fraction is then
519 topographically forced. If the surface of the ice is level when ponds drain, the ice surface will be
520 uniformly above sea level, leaving pond-free ice. If, however, snow dunes or differential melt creates
521 roughness on the surface, some of the surface will protrude from the ocean significantly and other areas
522 will not, creating the possibility for ponds to remain at sea level. If topography is the primary driver of
523 pond fraction, we expect FYI pond coverage late in the year would be highly variable: low on FYI that
524 remains smooth, higher on moderately rough FYI, and lower again on the roughest FYI (see Popović et
525 al., (2018) for more discussion). Given the range of outcomes and range of snow/ice topography on FYI,
526 there would not be a characteristic relationship between pond coverage on FYI and adjacent MYI.

Deleted: multiyear ice

Deleted: .

Deleted: thicker FYI

Deleted: the more of the level surface sits above freeboard

Deleted: (Eicken and Perovich as well)

Deleted: variation of

Formatted: Not Highlight

Formatted: Not Highlight

Deleted: (

Formatted: Not Highlight

Field Code Changed

Deleted: a

Deleted:)

Deleted:

Deleted: The

Deleted: prevalence

Deleted: of these two very different types of behavior

Deleted: is

Deleted: ing

Field Code Changed

Deleted: ,

Deleted: divergent

Deleted: pond behavior

Deleted: .

Deleted: subtle

Formatted: Not Highlight

Deleted: powerful

Deleted: , likely

Formatted: Not Highlight

549 Examining the pond coverage in more detail provides evidence that the range of possible melt states
550 is larger on FYI than it is on MYI. In other words, FYI exhibits all possible states between low and high
551 coverage, while MYI pond fraction typically exists within a small window. Returning to the boxplots in
552 Fig. 7, note the larger interquartile range (IQR) of the first-year flights versus the multiyear flights. If we
553 were to accept the traditional hypothesis that all FYI had high pond cover, we would expect the FYI to
554 have a higher median but a similar IQR. However, this is not the case. These observations suggest pond
555 cover on FYI is highly variable, and only in a subset of circumstances does the ice exhibit the expected
556 higher pond fraction. Examples of each behavior are included in Fig. 8. The traditional understanding of
557 melt pond evolution on FYI, where flat undeformed ice allows melt water to spread horizontally and
558 create large areas of pond covered ice is often observed on landfast ice or ice attached to a multiyear
559 floe (e.g. Barber and Yackel, 1999; Derksen et al., 1997; Fetterer and Untersteiner, 1998b; Uttal et al.,
560 2002). For example, Fig. 6b shows a refrozen lead between two MYI floes, where the pond fraction is
561 significantly higher on the flat FYI than on either of the adjoining MYI floes. Along the July 19, 2016
562 transect many of the smaller (less than 200m diameter) freely floating floes of flat FYI exhibited little to
563 no pond cover late in the melt season (as seen in Fig. 10d). We also note many examples of floes that
564 are pond free along their edges, such as in Fig. 10c, and floes that exhibit nearly complete pond
565 coverage (such as 10b,g,h). This dataset, therefore, helps establish that no simple relationship between
566 FYI and MYI ponding exists, and presents the possibility that the transition to FYI is not causing uniformly
567 higher melt pond fraction, as has been expected. Due to the temporal variability in pond evolution,
568 complete timeseries datasets are needed to fully analyze the relationship between MPF and ice age. The
569 highly variable nature of FYI ponding is, however, regionally coherent, strongly suggesting that the
570 history of conditions the ice is subject to governs ponding. Connecting conditions to pond prevalence is
571 therefore a topic worthy of investigation for better understanding FYI albedo feedbacks.

572 5 Conclusion

573 A new dataset quantifying sea ice surface fractions observed in Operation IceBridge DMS imagery has
574 been created using the recently developed OSSP algorithm. This dataset classifies the surface coverage
575 into four categories. During the melt season these categories are: 1) snow or thick ice, 2) dark or thin
576 ice, 3) melt ponds and submerged ice, and 4) open water. In freezing conditions, the categories become
577 1) snow or thick ice, 2) dark or thin ice, 3) open water, and 4) ridge shadows. The dataset allows for the
578 investigation of sea ice surface type distributions along OIB transects and opens the door for new
579 studies, both by analysing this dataset in isolation (as demonstrated here), and by combining it with
580 coincident OIB datasets such as ice thickness or ice roughness. This dataset is available at the NSDIC for
581 community use. Future improvements to this dataset should include work towards a more sophisticated
582 haze removal algorithm to apply to the OIB optical images. This will increase accuracy and increase the
583 fraction of images that can be successfully processed.

584 We have investigated snapshots of melt pond coverage differences between FYI and MYI in the
585 Beaufort/Chukchi Sea region for 2016 and the Lincoln Sea for 2017. Our results support previous
586 findings that FYI can have lower pond fraction than MYI under similar forcing conditions. While the
587 results presented herein cannot definitively confirm or refute the hypothesis that FYI has higher mean
588 pond fraction than MYI, the high variability in FYI pond fraction over large regions suggests that the
589 general rule of thumb that FYI should have higher ponding than MYI is too simplistic. Furthermore, the

Deleted: first-year ice

Deleted: multiyear ice

Deleted: first-year ice

Deleted: multiyear ice

Formatted: Not Highlight

Deleted: <

Deleted:

Deleted: F

Formatted: Not Highlight

Deleted: often

Formatted: Not Highlight

Deleted: that

Deleted: will be

Deleted: ()

Deleted: by X and Y

Deleted: the

603 ~~finding that FYI~~ exhibits much larger variance ~~over its temporal~~ evolution ~~indicates that~~ there is not one
604 path that defines the typical ~~pond coverage~~ ~~changes~~. ~~We did not find sufficient evidence that there is a~~
605 ~~strict duality in FYI pond evolution either, and we~~ suggest future process studies investigate the
606 mechanisms that drive FYI towards high or low pond fraction and specifically note that time-series
607 image observations and/or field studies may be necessary to unravel this question. The different
608 trajectories that pond development can apparently take on FYI may have large impacts on sea ice
609 modelling efforts, through albedo feedbacks. Furthermore, we suggest combining this new melt pond
610 dataset with data available from the IceBridge Airborne Topographical Mapper to determine the
611 relationship between sea ice topography and melt pond formation.

612

613 *Data and Code Availability.* The OSSP algorithm code is available on github
614 (<https://github.com/wrightni/ossps>) and the release for this manuscript is archived at zenodo (DOI:
615 10.5281/zenodo.3551033). The pond free detection algorithm will be archived at zenodo prior to
616 publication and is available at github (https://github.com/wrightni/pondfree_detection) during review.
617 Raw Operation IceBridge DMS imagery is available from the National Snow and Ice Data Center
618 (<https://doi.org/10.5067/OZ6VNOPMPRJO>). OSSP generated results are ~~also~~ archived at the NSDIC,
619 (<https://doi.org/10.5067/1LI57H56EB7G>).

620

621 *Author Contributions.* NW was responsible for writing the original draft, creating the data visualizations,
622 review and editing of the manuscript, designing and testing the OSSP software, conceptualization and
623 programming of the pond-free detection algorithm, and formal analysis of the OSSP generated results.
624 CP was responsible for initiating the study, contributing to writing and editing the manuscript, and
625 contributing to methodology and result analysis. SM was responsible for implementing the OSSP
626 software on NASA's Pleiades system, monitoring data processing, and data archiving. RB was responsible
627 for funding acquisition and supervision for the Ames Research Center team and for review and editing of
628 the manuscript draft.

629

630 *Conflicts of Interest.* The authors declare that they have no conflicts of interest.

631

632 *Acknowledgements.* The authors would like to thank NASA's AIST Program whose funding enabled this
633 research. The image processing for this work was carried out on NASA's Advanced Supercomputing
634 Pleiades system.

Deleted: a common hypothesis regarding the characteristics of melt pond development on FYI vs MYI and discovered evidence that it may be unsupported. FYI does not necessarily develop larger melt pond fractions than multiyear ice, even under the same atmospheric forcing conditions. We have presented additional evidence that first-year sea ice

Deleted: ; where

Deleted: behaviour

Deleted: evolution of

Deleted: W

Deleted: being uploaded and

Deleted:

Deleted: and will be available prior to publication of this manuscript...

649 **References**

- 650 Barber, D. G. and Yackel, J.: The physical, radiative and microwave scattering characteristics of melt
651 ponds on Arctic landfast sea ice, *Int. J. Remote Sens.*, 20(10), 2069–2090,
652 doi:10.1080/014311699212353, 1999.
- 653 Curry, J. A., Schramm, J. L. and Ebert, E. E.: Sea ice-albedo climate feedback mechanism, *J. Clim.*, 8(2),
654 240–247, doi:10.1175/1520-0442(1995)008<0240:SIACFM>2.0.CO;2, 1995.
- 655 De, K. and Masilamani, V.: Image Sharpness Measure for Blurred Images in Frequency Domain, *Procedia*
656 *Eng.*, 64, 149–158, doi:10.1016/J.PROENG.2013.09.086, 2013.
- 657 Derksen, C., Piwowar, J. and LeDrew, E.: Sea-Ice Melt-Pond Fraction as Determined from Low Level
658 Aerial Photographs, *Arct. Alp. Res.*, 29(3), 345–351, doi:10.1080/00040851.1997.12003254, 1997.
- 659 Dominguez, R.: IceBridge DMS L0 Raw Imagery, Version 1, , doi:10.5067/UMFN22VHGGMH, 2010.
- 660 Eicken, H., Grenfell, T. C., Perovich, D. K., Richter-Menge, J. A. and Frey, K.: Hydraulic controls of summer
661 Arctic pack ice albedo, *J. Geophys. Res. C Ocean.*, 109(8), doi:10.1029/2003JC001989, 2004a.
- 662 Fetterer, F. and Untersteiner, N.: Observations of melt ponds on Arctic sea ice, *J. Geophys. Res. Ocean.*,
663 103(C11), 24821–24835, doi:10.1029/98JC02034, 1998.
- 664 Hanesiak, J. M., Barber, D. G. and Flato, G. M.: Role of diurnal processes in the seasonal evolution of sea
665 ice and its snow cover, *J. Geophys. Res. Ocean.*, 104(C6), 13593–13603, doi:10.1029/1999JC900054,
666 1999.
- 667 Huang, W., Lu, P., Lei, R., Xie, H. and Li, Z.: Melt pond distribution and geometry in high Arctic sea ice
668 derived from aerial investigations, *Ann. Glaciol.*, 57(73), 105–118, doi:10.1017/aog.2016.30, 2016.
- 669 Hunke, E. C., Hebert, D. A. and Lecomte, O.: Level-ice melt ponds in the Los Alamos sea ice model, *CICE,*
670 *Ocean Model.*, 71, 26–42, doi:10.1016/j.ocemod.2012.11.008, 2013.
- 671 Landy, J., Ehn, J., Shields, M. and Barber, D.: Surface and melt pond evolution on landfast first-year sea
672 ice in the Canadian Arctic Archipelago, *J. Geophys. Res. Ocean.*, 119(5), 3054–3075,
673 doi:10.1002/2013JC009617, 2014.
- 674 Miao, X., Xie, H., Ackley, S., Perovich, D. and Ke, C.: Object-based detection of Arctic sea ice and melt
675 ponds using high spatial resolution aerial photographs, *Cold Reg. Sci. Technol.*, 119, 211–222,
676 doi:10.1016/j.coldregions.2015.06.014, 2015.
- 677 Morassutti, M. P. and Ledrew, B. F.: Albedo and depth of melt ponds on sea-ice, *Int. J. Climatol.*, 16(7),
678 817–838, doi:10.1002/(SICI)1097-0088(199607)16:7<817::AID-JOC44>3.0.CO;2-5, 1996.
- 679 Perovich, D. and Polashenski, C.: Albedo evolution of seasonal Arctic sea ice, *Geophys. Res. Lett.*, 39(8),
680 n/a-n/a, doi:10.1029/2012GL051432, 2012.
- 681 Perovich, D., Grenfell, T., Richter-Menge, J., Light, B., Tucker, W. and Eicken, H.: Thin and thinner: Sea ice
682 mass balance measurements during SHEBA, *J. Geophys. Res. Ocean.*, 108(C3),
683 doi:10.1029/2001JC001079@10.1002/(ISSN)2169-9291.SHEBA1, 2003.
- 684 Perovich, D. K.: Aerial observations of the evolution of ice surface conditions during summer, *J. Geophys.*
685 *Res.*, 107(C10), 8048, doi:10.1029/2000JC000449, 2002a.

686 Perovich, D. K.: Aerial observations of the evolution of ice surface conditions during summer, *J. Geophys. Res.*, 107(C10), 8048, doi:10.1029/2000JC000449, 2002b.

688 Polashenski, C., Perovich, D. and Courville, Z.: The mechanisms of sea ice melt pond formation and evolution, *J. Geophys. Res. Ocean.*, 117(C1), n/a-n/a, doi:10.1029/2011JC007231, 2012.

690 Polashenski, C., Perovich, D. K., Frey, K. E., Cooper, L. W., Logvinova, C. I., Dadic, R., Light, B., Kelly, H. P., Trusel, L. D. and Webster, M.: Physical and morphological properties of sea ice in the Chukchi and Beaufort Seas during the 2010 and 2011 NASA ICESCAPE missions, *Deep Sea Res. Part II Top. Stud. Oceanogr.*, 118, 7–17, doi:10.1016/J.DSR2.2015.04.006, 2015.

694 Polashenski, C., Golden, K., Perovich, D., Skillingstad, E., Arnsten, A., Stwertka, C. and Wright, N.: Percolation blockage: A process that enables melt pond formation on first year Arctic sea ice, *J. Geophys. Res. Ocean.*, 122(1), 413–440, doi:10.1002/2016JC011994, 2017.

697 Popović, P., Cael, B. B., Silber, M. and Abbot, D. S.: Simple Rules Govern the Patterns of Arctic Sea Ice Melt Ponds, *Phys. Rev. Lett.*, 120(14), 148701, doi:10.1103/PhysRevLett.120.148701, 2018.

699 Serreze, M. C., Barrett, A. P., Stroeve, J. C., Kindig, D. N. and Holland, M. M.: The emergence of surface-based Arctic amplification, *Cryosphere*, 3(1), 11–19, doi:10.5194/tc-3-11-2009, 2009.

701 Stroeve, J. C., Serreze, M. C., Holland, M. M., Kay, J. E., Malanik, J. and Barrett, A. P.: The Arctic's rapidly shrinking sea ice cover: a research synthesis, *Clim. Change*, 110, 1005–1027, doi:10.1007/s10584-011-0101-1, 2012.

704 Uttal, T., Curry, J. A., Mcphee, M. G., Perovich, D. K., Moritz, R. E., Maslanik, J. A., Guest, P. S., Stern, H. L., Moore, J. A., Turenne, R., Heiberg, A., Serreze, M. C., Wylie, D. P., Persson, O. G., Paulson, C. A., Halle, C., Morison, J. H., Wheeler, P. A., Makshtas, A., Welch, H., Shupe, M. D., Intrieri, J. M., Stamnes, K., Lindsey, R. W., Pinkel, R., Pegau, W. S., Stanton, T. P., Grenfeld, T. C., Uttal, T., Curry, J. A., Mcphee, M. G., Perovich, D. K., Moritz, R. E., Maslanik, J. A., Guest, P. S., Stern, H. L., Moore, J. A., Turenne, R., Heiberg, A., Serreze, M. C., Wylie, D. P., Persson, O. G., Paulson, C. A., Halle, C., Morison, J. H., Wheeler, P. A., Makshtas, A., Welch, H., Shupe, M. D., Intrieri, J. M., Stamnes, K., Lindsey, R. W., Pinkel, R., Pegau, W. S., Stanton, T. P. and Grenfeld, T. C.: Surface Heat Budget of the Arctic Ocean, *Bull. Am. Meteorol. Soc.*, 83(2), 255–275, doi:10.1175/1520-0477(2002)083<0255:SHBOTA>2.3.CO;2, 2002.

713 van der Walt, S., Schönberger, J. L., Nunez-Iglesias, J., Boulogne, F., Warner, J. D., Yager, N., Gouillart, E. and Yu, T.: scikit-image: image processing in Python, *PeerJ*, 2, e453, doi:10.7717/peerj.453, 2014.

715 Webster, M. A., Rigor, I. G., Perovich, D. K., Richter-menge, J. A., Polashenski, C. M. and Light, B.: Seasonal evolution of melt ponds on Arctic sea ice, *J. Geophys. Res. Ocean.*, 120(9), 1–15, doi:10.1002/2015JC011030, 2015.

718 Weeks, W.: *On Sea Ice*, University of Alaska Press. [online] Available from: <https://books.google.de/books?id=9555O6WzUL8C> (Accessed 18 January 2018), 2010.

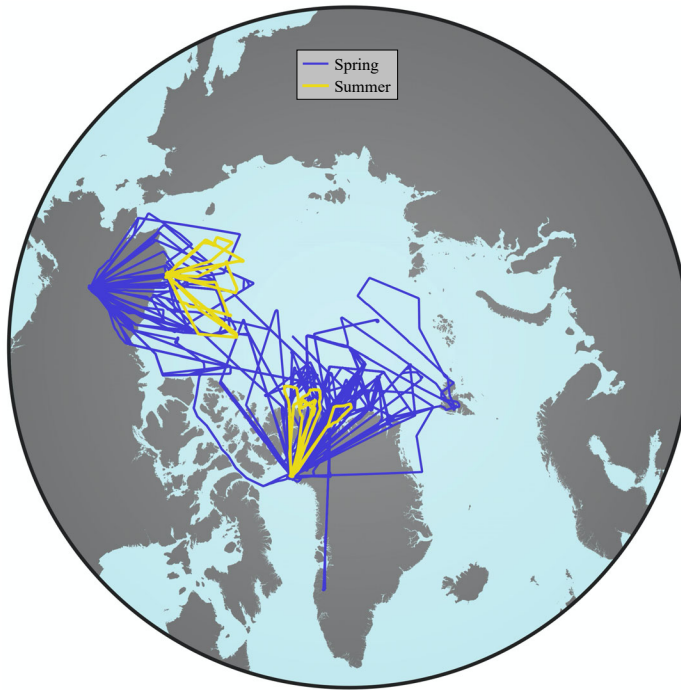
720 Wright, N. and Polashenski, C.: Open-source algorithm for detecting sea ice surface features in high-resolution optical imagery, *Cryosphere*, 12(4), 1307–1329, doi:10.5194/tc-12-1307-2018, 2018.

722

723

724 **Figures**

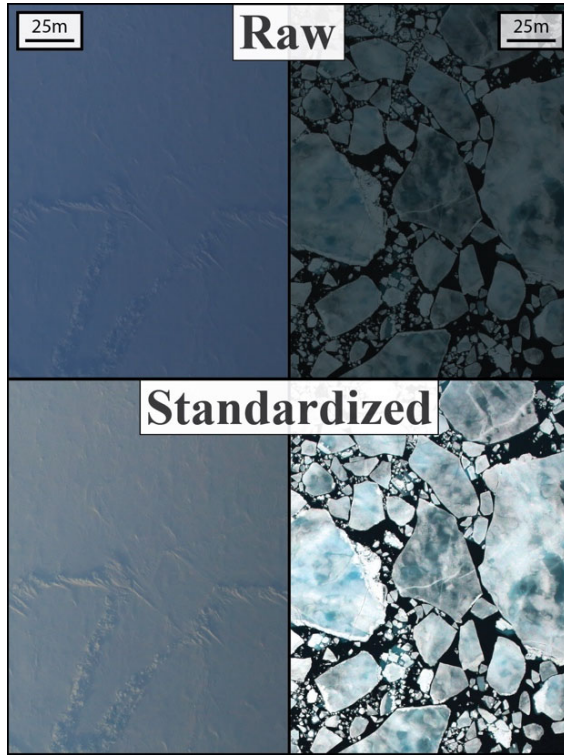
725



726

727 **Figure 1. Plot of all flights processed with OSSP, colored by the melt conditions during the flight. Spring freezing conditions in**
728 **blue, and summer melting conditions in yellow.**

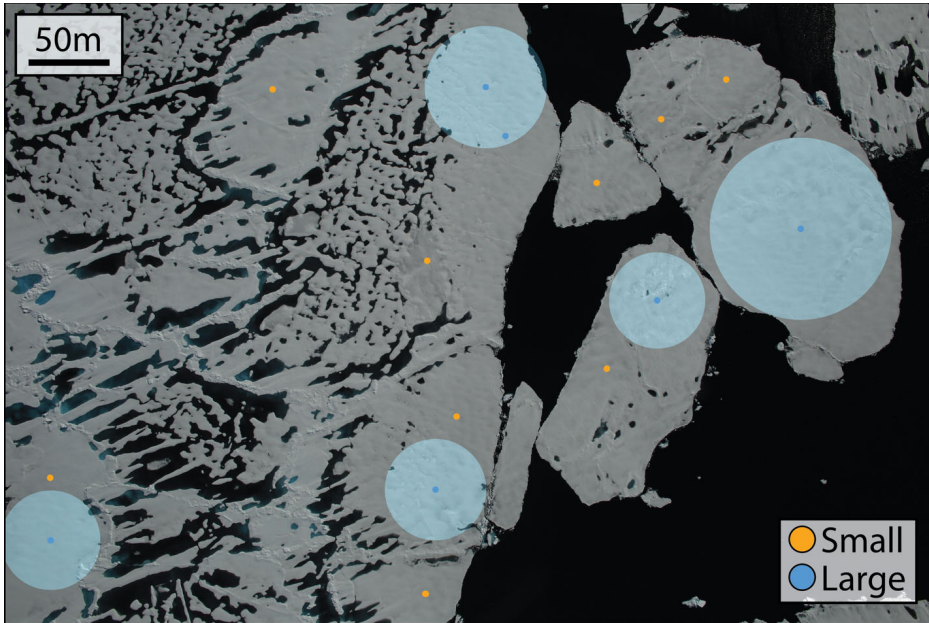
729



730

731 **Figure 2. Demonstration of the image preprocessing steps. The raw images (top) have poor surface illumination and a blue**
732 **hue, both of which have been removed in the standardized images (bottom).**

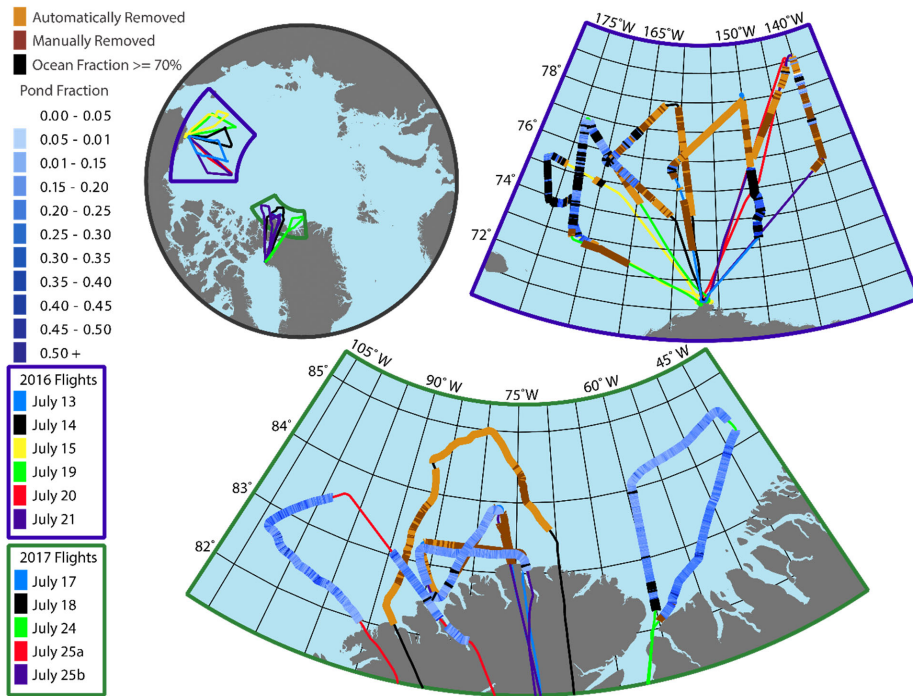
733



734

735 Figure 3. Example of the pond free region detection. Pond free regions are marked by small colored dots, where blue dots
736 indicate the larger regions and orange indicates the smaller ones. Translucent blue circles are drawn with a radius equal to
737 the size of the detected large regions. Blue dots without a translucent circle were merged with a neighboring region.

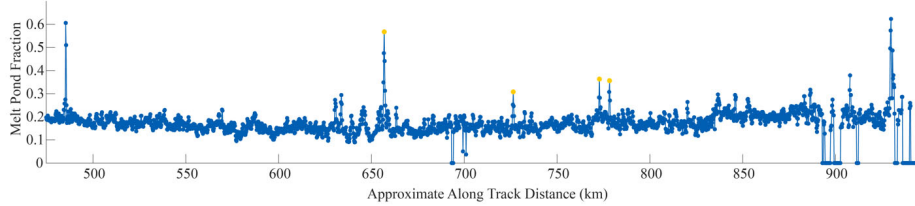
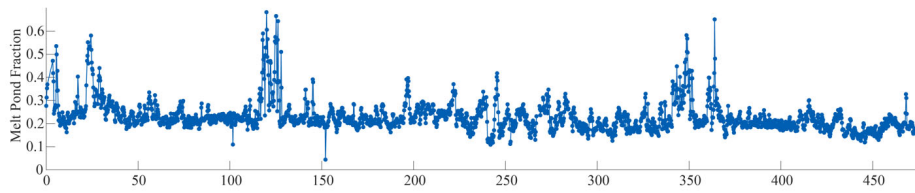
738



739

740 **Figure 4. Melt pond fraction along OIB summer transects. Automatically and manually removed images are indicated by**
 741 **orange and red, respectively. 2016 flights were more prone to haze obscuring the ice surface and therefore have more**
 742 **deleted images.**

743



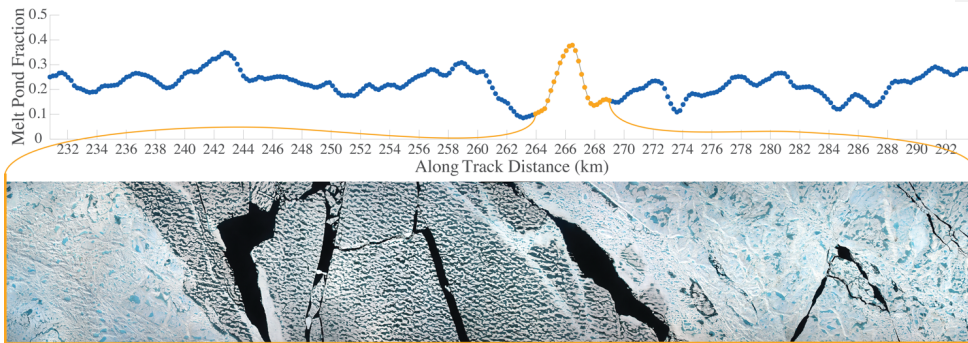
744

745 **Figure 5. Melt pond fraction along track for flight July 24, 2017. The four orange highlighted points represent areas where**
 746 **there was a large blue pond on the multiyear ice that occupied a large fraction of the image. See Fig. 11d for an example of**
 747 **this feature.**

748

749

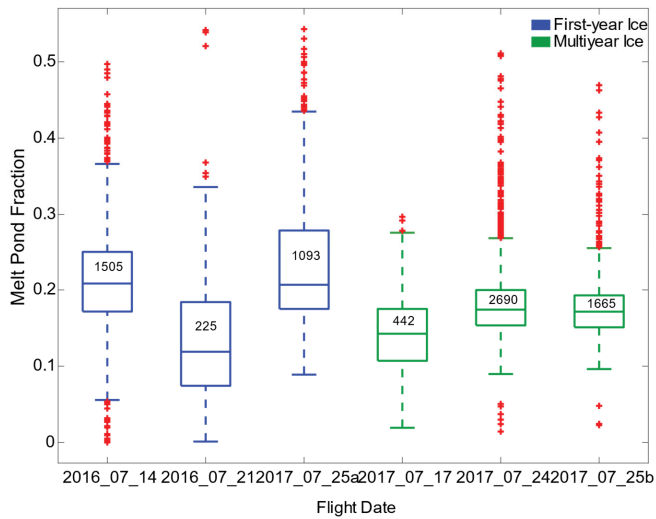
750



751

752 **Figure 6. Melt pond fraction along a several kilometer section of the July 24, 2017 flight. The orange highlighted region is**
 753 **depicted as a series of stitched together DMS images that show a first-year inclusion between two multiyear floes.**

754

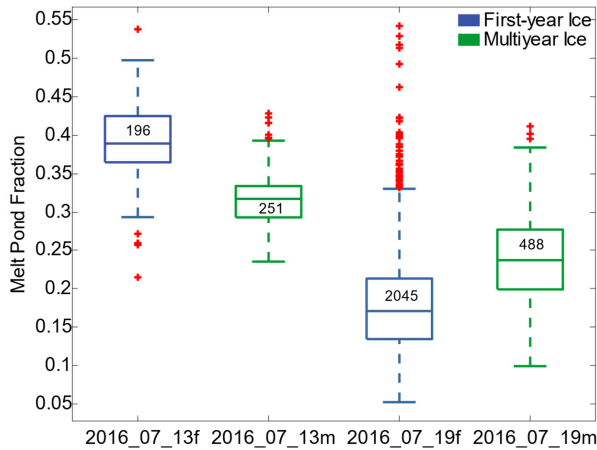


755

756
757
758

Figure 7. Melt pond statistics from summer OIB flight which contained only a single ice type. Blue corresponds to first-year ice statistics, green to multiyear ice statistics, and red crosses indicate outliers. The number of image frames used to calculate statistics for each flight is included inside the box. The approximate area of each image frame is 0.25 km².

Formatted: Caption
Deleted:
Deleted: ¶
Deleted: ¶



759

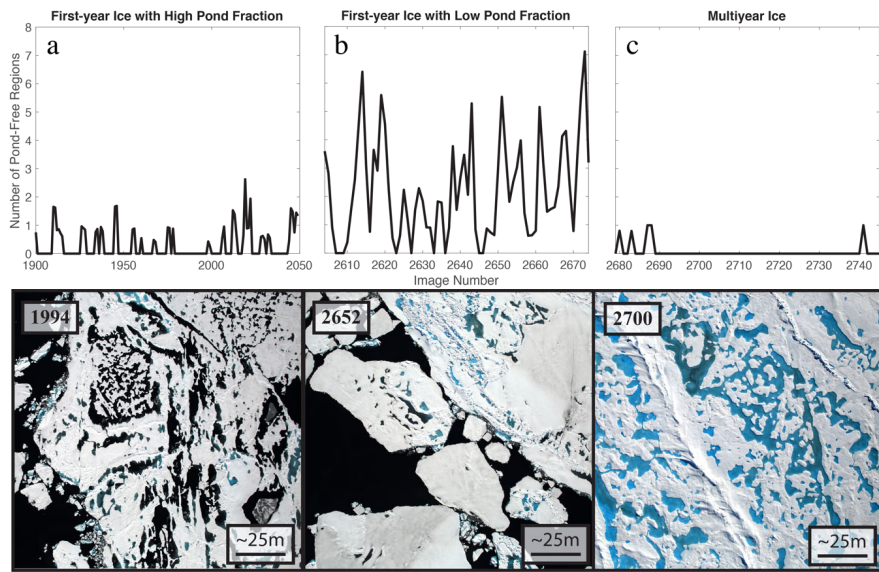
760
761
762
763

Figure 8. Melt pond statistics from two flights that contain both first-year and multiyear ice. In the July 13 case, multiyear ice has a lower pond fraction, while in the July 19 case the first-year ice has a lower pond fraction. Blue corresponds to first-year ice statistics, green to multiyear ice statistics, and red crosses indicate outliers. The number of image frames used to calculate statistics for each flight is included inside the box. The approximate area of each image frame is 0.25 km².

Deleted:

769

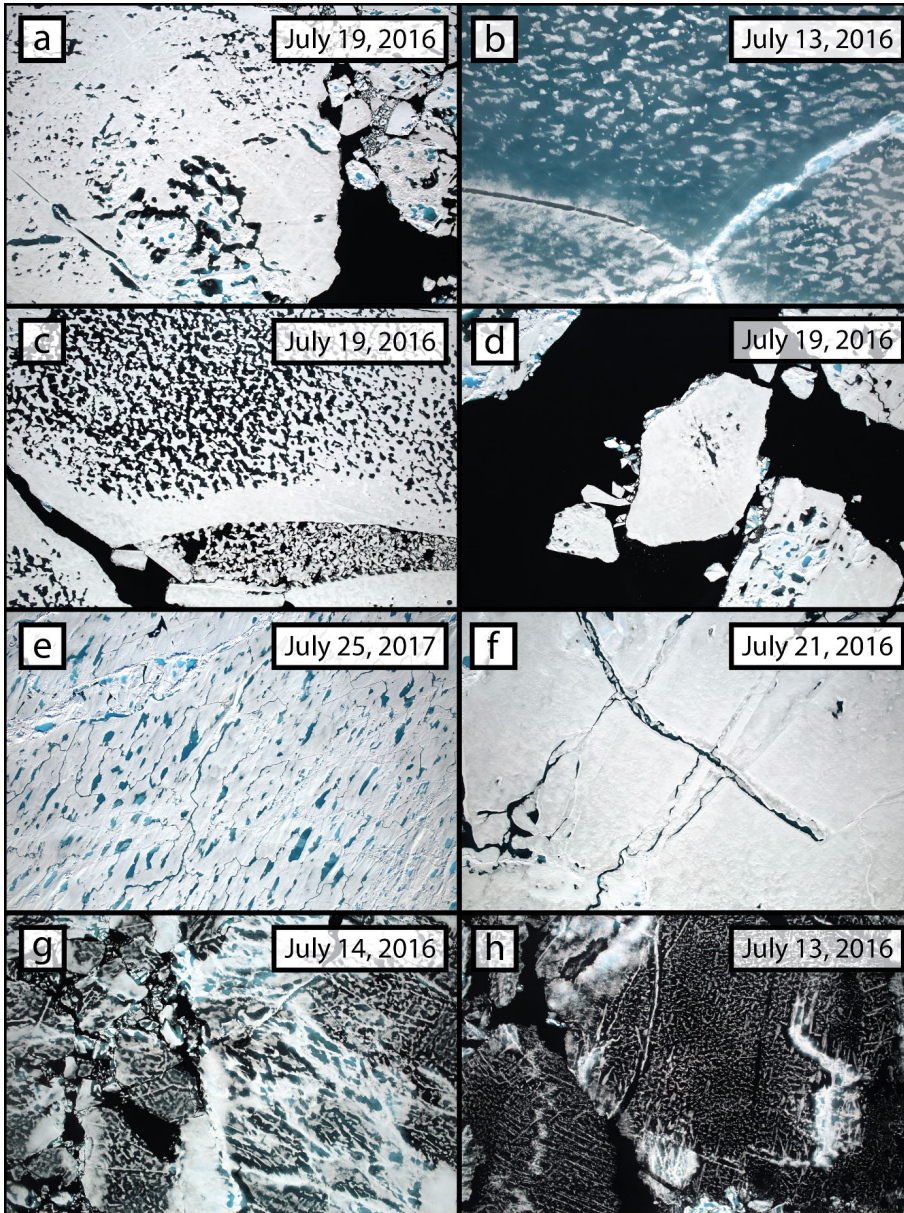
770



771

772 Figure 9. Number of pond-free regions on several regions of sea ice observed during the July 19, 2016 flight (top) and a
773 sample image representing that region of ice (bottom).

774

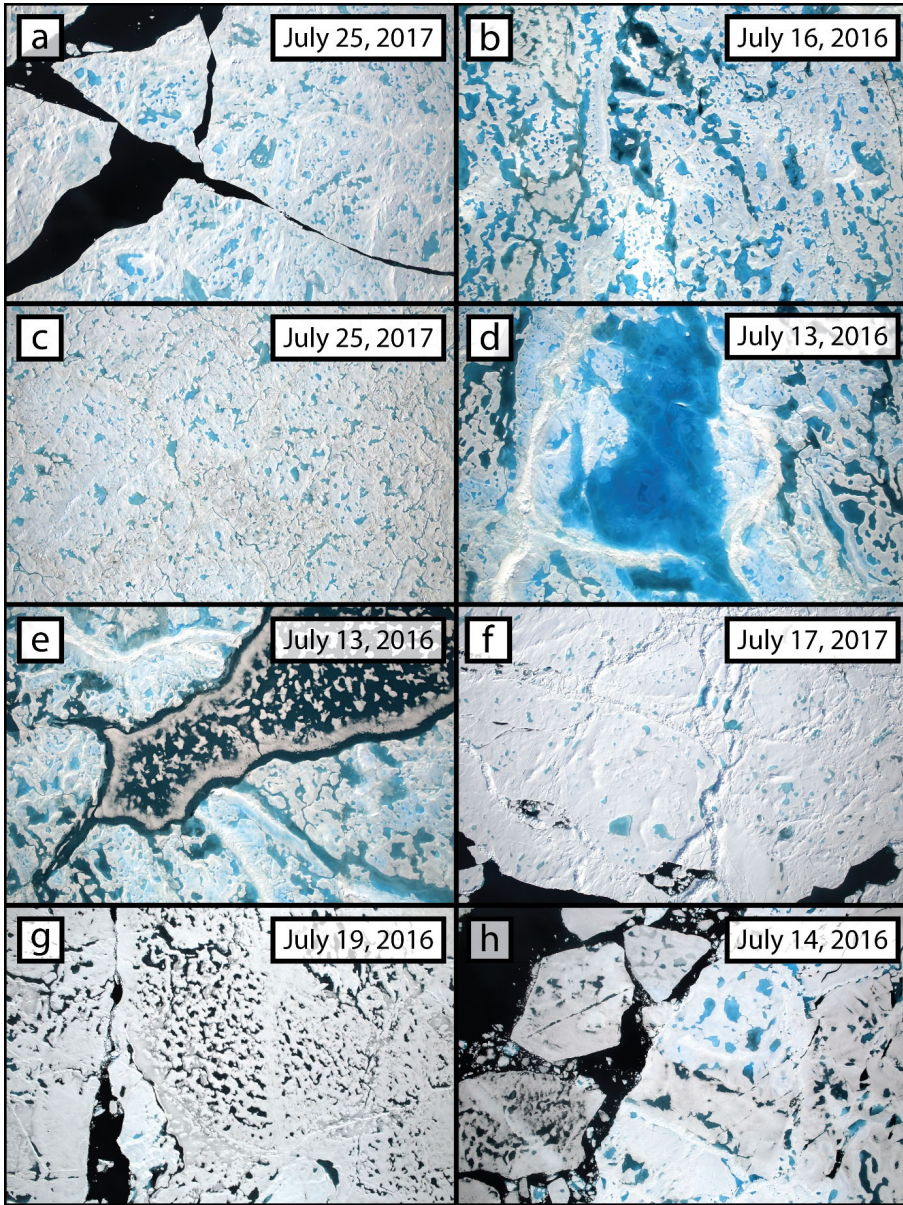


775

776

777

Figure 10. Exhibits of sea ice surface features as seen in the DMS dataset. Each panel is a full IceBridge image, and while flight altitude affects image resolution, each scene is approximately 600 m by 400 m. See text for full description of each frame.



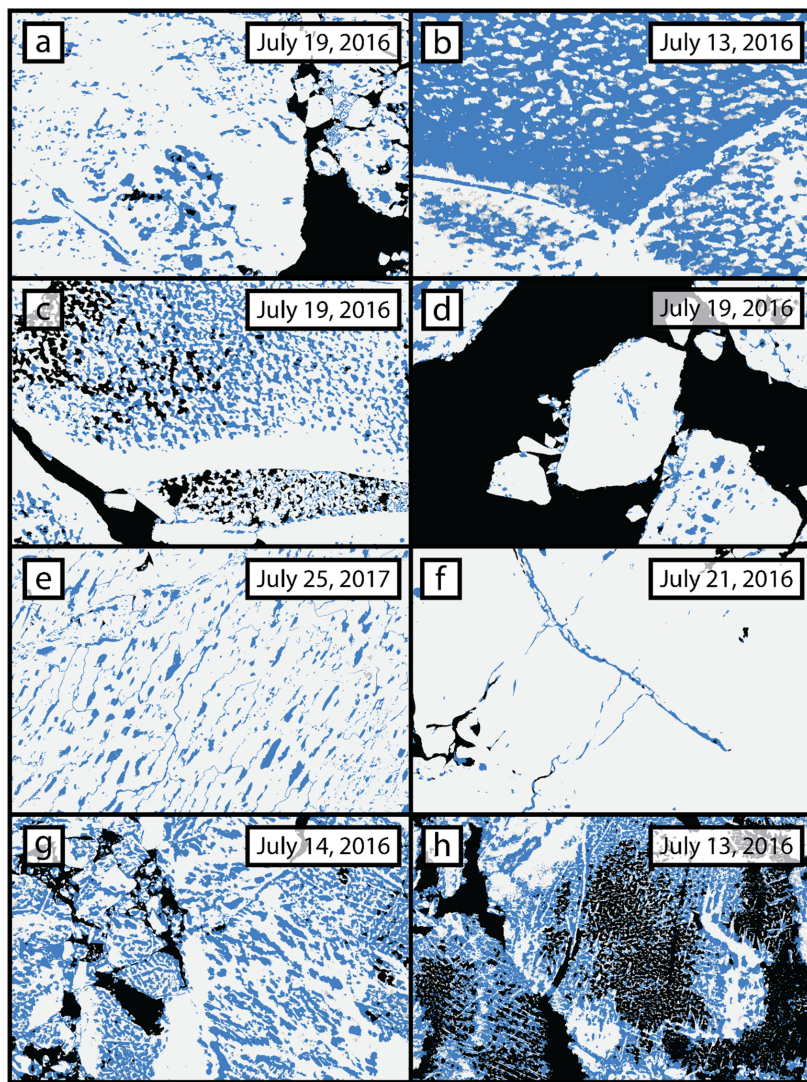
778

779

780

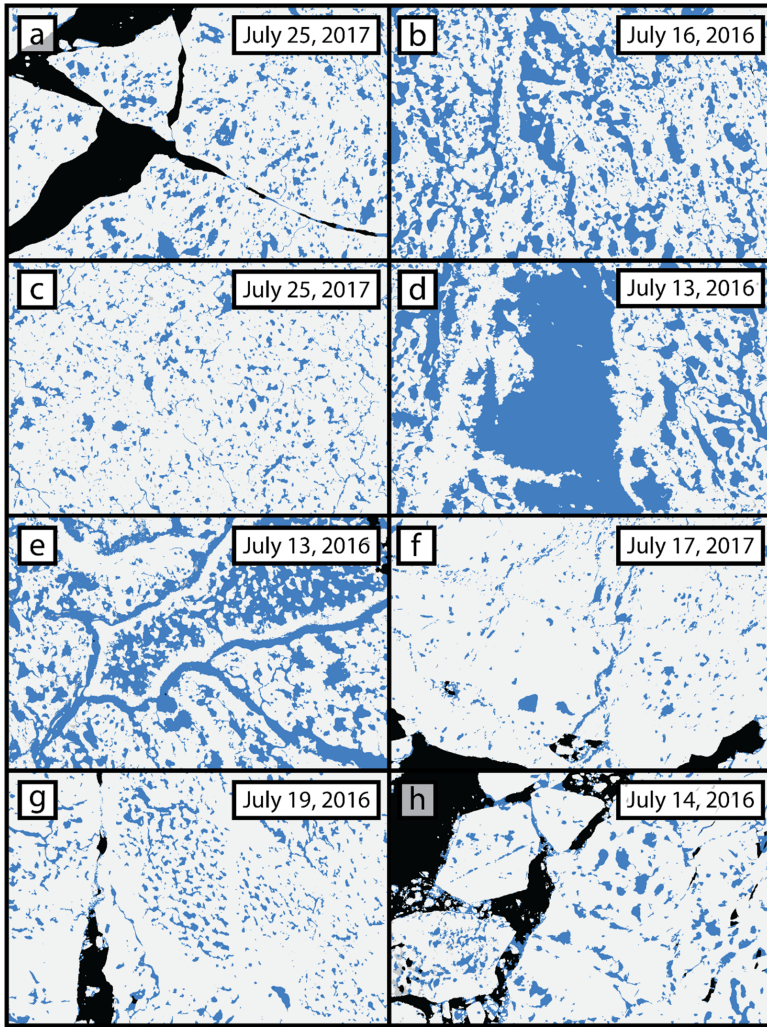
Figure 11. Exhibits of sea ice surface features as seen in the DMS dataset. Each panel is a full IceBridge image, and while flight altitude affects image resolution, each scene is approximately 600 m by 400 m. See text for full description of each frame.

781 [Supplemental Figures:](#)



782

783 [Figure S1. Classified versions of the images shown in Figure 10. White regions are snow/ice, blue regions](#)
784 [are melt ponds or submerged ice, and black regions are open water.](#)



785

786 [Figure S2](#). Classified versions of the images shown in [Figure 11](#). White regions are snow/ice, blue regions
 787 are melt ponds are submerged ice, black regions are open water.

Formatted: Normal